Breaking Network Connectivity Leads to Ultralow Thermal Conductivities in Fully Dense Amorphous Solids: Supplementary Material

Jeffrey L. Braun, Ashutosh Giri, John T. Gaskins, and Patrick E. Hopkins
Department of Mechanical and Aerospace Engineering,
University of Virginia, Charlottesville, VA 22904, USA

Sean W. King
Intel Corporation, Logic Technology Development, 5200 NE Elam Young Parkway, Hillsboro, Oregon 97124

Masanori Sato, Takemasa Fujiseki, and Hiroyuki Fujiwara
Department of Electrical, Electronic and Computer Engineering, Gifu University, 1-1 Yanagido, Gifu 501-1193, Japan

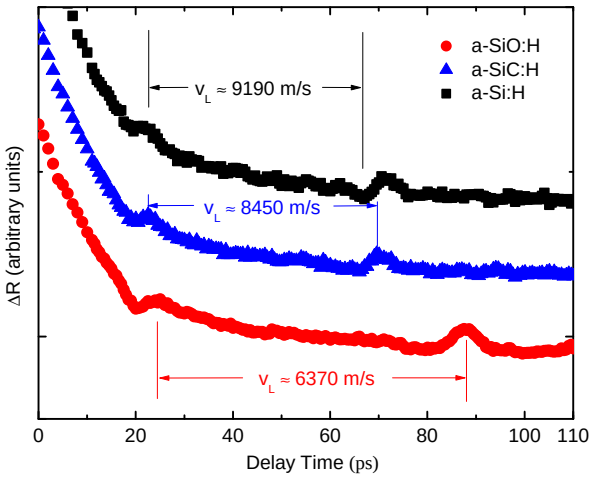

FIG. S1. Change in reflectivity vs. probe delay time. Longitudinal sound speed is derived by determining the time between troughs corresponding the time for a strain wave to propagate across the aluminum transducer layer and reflecting from the Al/a:H interface and the peak/trough corresponding to the strain wave propagating across the a-Si[O/C]:H layer and reflecting at the a-Si[O/C]:H/c-Si interface.

I. DETERMINATION OF SOUND SPEED

We used two independent methods to determine longitudinal and transverse sound speeds for these samples. The first, nano-indentation, is described in Ref. [1]. The second, picosecond acoustics uses the picosecond delay time regime in our time-domain thermoreflectance signal to measure longitudinal sounds speed in the a-Si[O/C]:H films [2–4]. During this technique, the heating event induced by the incident pump beam excitation creates a strain wave that propagates across the aluminum and a-Si[O/C]:H film at each layer's sound speed. Upon reaching an interface, the strain wave is partially reflected; this reflectance, upon reaching the aluminum surface, changes the reflectance signal measured via the probe beam in the picosecond time regime beyond the heating event. Thus, we measure the increase or decrease in amplitude of measured reflectivity (which depends on the relative magnitude of acoustic impedance between layers in each sample) to determine the time it takes this strain wave to propagate across each film. This propagation time, together with the thickness of the films, allows us to determine the longitudinal sound speed of each a-Si[O/C]:H film.

Figure S1 displays the reflectivity data measured during TDTR up to 110 picoseconds beyond the heating event for three representative samples. The first local maximum in reflectivity results from the partially reflected strain wave from the Al/a-Si[O/C]:H interface reaching the surface. Because the acoustic impedance of the Al film is lower than that of the a-Si[O/C]:H layer, the magnitude of reflectivity measured at the sample surface is lowered. Hence, when measuring the propagation time of this strain wave, we take the time value associated with the local maximum of our signal caused by this event. In the case of the a-Si:H film, the acoustic impedance of the a-Si:H layer is higher than that of the Si substrate; thus, when determining the time associated with the strain wave partially reflecting from the aSi:H/c-Si interface, we take the time corresponding to the local minimum of the reflectance signal. In the case of the a-SiC:H and a-SiO:H, the acoustic impedances of these films are lower than that of the c-Si substrate, so that the time associated with the strain wave partially reflecting from the a-SiC:H/c-Si or a-SiO:H/c-Si interface corresponds to the local maximum. We note that picosecond acoustics is often used in TDTR to measure thickness of the metal transducer layer. In this case, we do the same to confirm the aluminum layer is 80 $\pm$3 nm; this has the added benefit of providing a calibration for the determination of a:Si[O/C]:H film sound speeds.

Using the elastic modulus from nano-indentation, we derive longitudinal sound speed from a continuum mechanics approach. For linear elastic isotropic materials, as is the case for most amorphous films, the elastic and shear moduli can be related to the longitudinal and transverse sound speeds in a material through simple analytical expressions: $C_{11} = \rho v_L^2$ and $E = C_{11} + 2C_{12}^2/(C_{11} + C_{12})$, where C_{11} and C_{12} are elastic stiffness constants relating stress and strain, ρ is mass density, and E is elastic modulus measured via nano-indentation. Using the relation for Poisson's ratio given by $\nu = C_{12}/(C_{11} + C_{12})$, the

following relations can be formed

$$v_L = \sqrt{\frac{E(1-\nu)}{\rho(1+\nu)(1-2\nu)}} \tag{S1}$$

$$v_T = \sqrt{\frac{G}{\rho}} = \sqrt{\frac{E}{2\rho(1+\nu)}} \tag{S2}$$

where v_T is transverse sound speed and G is the shear modulus. Under the assumption that ν is that of amorphous silicon, 0.22 [5], both longitudinal and transverse sound speeds are derived using these independent techniques to find excellent agreement between them.

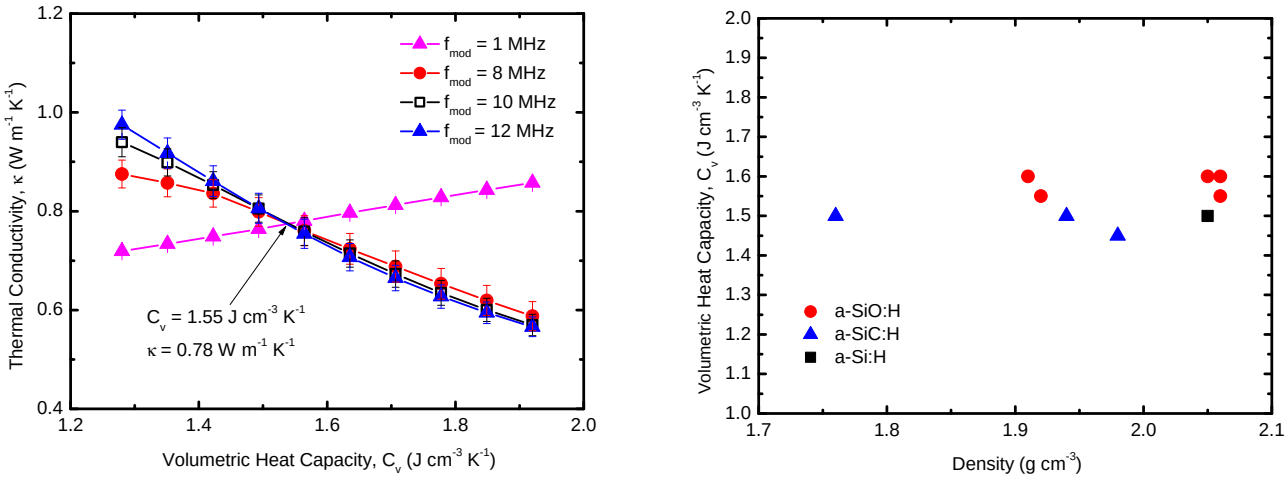

(a) Thermal conductivity vs. volumetric heat capacity

(b) Density vs. Heat Capacity

FIG. S2. (a) Thermal conductivity as fitted in TDTR analysis vs. input heat capacity. The true values for thermal conductivity and heat capacity are determined by the intersection of profiles observed for different modulation frequencies having varying sensitivities to heat capacity. (b) Heat capacity as determined by TDTR vs. density. Heat Capacity does not vary significantly among samples.

II. MEASURING HEAT CAPACITY AND THERMAL CONDUCTIVITY SIMULTANEOUSLY

While we expect heat capacity to change negligibly among samples, to ensure this assumption does not effect the thermal conductivity measurements, we follow the procedure outlined by Liu et al.[6], analyzing TDTR data from different modulation frequencies with varying input values for heat capacity. Because the sensitivities to various parameters change with modulation frequency, the profile of fitted thermal conductivity as a function of assumed heat capacity varies significantly with heat capacity; this is observed in Fig. S2(a) for an a-SiO:H sample. The true values for thermal conductivity and heat capacity are determined by the intersection of these various profiles of thermal conductivity vs. heat capacity. As observed, different curves all converge to a single point; this is the reported value for thermal conductivity used in the main document. Following this procedure for all samples, the measured heat capacities are observed to remain relatively constant, as depicted in Fig. S2(b), which shows heat capacity as a function of density. Density is fixed to a small range of values to ensure that this volumetric heat capacity remains constant among films. This ensures that differences in thermal conductivity are not a result of heat capacity differences among films, as discussed in the main document. Uncertainty in density is roughly 0.1 g cm^{-3}. Since the measured thermal conductivity is obtained through a simultaneous fit with heat capacity, we can be assured that any uncertainty in density has no influence on reported values obtained through TDTR. For thermal conductivity values calculated via models in the manuscript, uncertainty in density translates to only 2.6% – 3.3% of thermal conductivity values.

[1] M. Sato, S. W. King, W. A. Lanford, P. Henry, T. Fujiseki, and H. Fujiwara, Journal of Non-Crystalline Solids **440**, 49 (2016).
[2] C. Thomsen, H. T. Grahn, H. J. Maris, and J. Tauc, Phys. Rev. B **34**, 4129 (1986).
[3] G. A. Antonelli, B. Perrin, B. C. Daly, and D. G. Cahill, MRS bulletin **31**, 607 (2006).
[4] D. Hondongwa, L. Olasov, B. Daly, S. King, and J. Bielefeld, Thin Solid Films **519**, 7895 (2011).
[5] L. B. Freund and S. Suresh, *Thin film materials: stress, defect formation and surface evolution* (Cambridge University Press, 2004).
[6] J. Liu, J. Zhu, M. Tian, X. Gu, A. Schmidt, and R. Yang, Review of Scientific Instruments **84**, 034902 (2013).